

# Saturation and Microsecond Gating of Current Indicate Depletion-induced Instability of the MaxiK Selectivity Filter

Indra Schroeder and Ulf-Peter Hansen

Department of Structural Biology, University of Kiel, 24098 Kiel, Germany

Patch clamp experiments on single MaxiK channels expressed in HEK293 cells were performed with a high temporal resolution (50-kHz filter) in symmetrical solutions with 50, 150, or 400 mM KCl and 2.5 mM CaCl<sub>2</sub> and 2.5 mM MgCl<sub>2</sub>. At membrane potentials > +100 mV, the single-channel current showed a negative slope resistance, concomitantly with a flickery block, which was not influenced by Ca<sup>2+</sup> or Mg<sup>2+</sup>. The analysis of the amplitude histograms by beta distributions revealed that current in this voltage range was reduced by two effects: rate limitation at the cytosolic side of the pore and gating with rate constants 10–20-fold higher than the cutoff frequency of the filter (i.e., dwell times in the microsecond range). The data were analyzed in terms of a model that postulates a coupling between both effects; if the voltage over the selectivity filter withdraws ions from the cavity at a higher rate than that of refilling from the cytosol, the selectivity filter becomes instable because of ion depletion, and current is interrupted by the resulting flickering. The fit of the IV curves revealed a characteristic voltage of 35 mV. In contrast, the voltage dependence of the gating factor *R*, i.e., the ratio between true and apparent single-channel current, could be fitted by exponentials with a characteristic voltage of 60 mV, suggesting that only part of the transmembrane potential is felt by the flux through the selectivity filter.

## INTRODUCTION

Ion channels in situ are not permanently open. Instead, they switch randomly, voltage or ligand controlled between conducting and nonconducting states. This so-called gating behavior is a major determinant of their physiological role, and malfunction of gating may lead to severe health problems (Lehmann-Horn and Jurkat-Rott, 1999; Proks et al., 2001, 2005). The loci and mechanisms of these gating processes are not yet clear in most cases, even though there are several promising approaches.

The N-terminal chain and ball mechanism (Armstrong et al., 1973), which actually is a finger in K<sup>+</sup> channels (Bentrop et al., 2001) and a hinged lid in Na<sup>+</sup> channels (Catterall, 2000), plays an important role in inactivation processes especially during action potentials of nerves (Catterall, 2000). Structural analysis has provided clear evidence for channel closing by the inner gate (Perozo et al., 1999; Liu et al., 2001) as mediated by bending of the S6 (TM2) helix (NaChBac, Zhao et al., 2004; KcsA and MthK, Jiang et al., 2002; *Shaker*, Del Camino et al., 2000; Del Camino and Yellen, 2001). An alternative mechanism of closing the inner gate is implemented by the N terminus in the virus-encoded Kcv channel (Tayefeh et al., 2007).

Gating by the selectivity filter is involved in very slow processes like C inactivation (Kiss et al., 1999). Even when low pH fully opens the inner gate of KcsA, slow gating can be observed that is related to voltage-

dependent E71–D80 interactions (Cordero-Morales et al., 2006a,b). Blunck et al. (2006) employed fluorescence measurements to prove that KcsA was really open when E71-related gating occurred. In GIRK, gating of the selectivity filter became obvious when the inner gate was locked in the open state by mutations (V188G, Yi et al., 2001). Involvement of the selectivity filter also in faster (or medium with respect to the rate constants found here) gating was found in Kir channels (Proks et al., 2001; Claydon et al., 2003; Xie et al., 2004). Furthermore, the occurrence of subconductance levels during channel opening and deactivation in the T442S mutant of *Shaker* (Zheng and Sigworth, 1998) was considered to be related to fast structural changes in the selectivity filter.

Here, we present a hypothesis that very fast gating of the selectivity filter may be involved in the generation of the negative slope of the apparent single-channel current/voltage relationship in MaxiK channels. A linear increase of the current with driving force (electrical potential and concentration gradient) is found only in the vicinity of the reversal potential. At higher negative and/or positive potentials, the measured (apparent) current may become independent of driving force (saturation) or may even start to decline with increasing driving force (negative slope or negative resistance).

Negative slopes in whole-cell data have been observed in out- and inward currents in different kinds of

Correspondence to Ulf-Peter Hansen: uphansen@zbm.uni-kiel.de

channels in plants (Beilby, 1985; Tester, 1988), animals (e.g., in Kir channels, Alagem et al., 2001; Murata et al., 2002; Yeh et al., 2005; in MaxiK, Cox et al., 1997; Ransom and Sontheimer, 2001), and viruses (Kang et al., 2004). Often its occurrence has been attributed to the interaction with divalent (e.g.,  $\text{Ba}^{2+}$  in Kir 2.1, Alagem et al., 2001; Murata et al., 2002;  $\text{Ca}^{2+}$  in MaxiK, Ransom and Sontheimer, 2001;  $\text{Mg}^{2+}$  in ROMK1, Lu and MacKinnon, 1994) or monovalent cations (e.g.,  $\text{Cs}^+$  in MaxiK, DeCoursey et al., 1996; or  $\text{Tl}^+$  in Kir2.1, Yeh et al., 2005). This started with the early observation of Bezanilla and Armstrong (1972) that the entry of  $\text{Na}^+$  or  $\text{Cs}^+$  into the  $\text{K}^+$  channel of the squid axon caused a negative slope.

Negative slopes were also found in single-channel records (DeCoursey et al., 1996; Cox et al., 1997; LeMasurier et al., 2001; Sørensen et al., 2001; Nimigean and Miller, 2002; Zhang et al., 2006; Pagliuca et al., 2007). As in the case of whole-cell records, an important role of blocking ions was documented in many studies. For instance, the presence of  $\text{Na}^+$  caused a negative slope in KcsA (Nimigean and Miller, 2002). In *Chara*, single-channel currents of the large  $\text{Ca}^{2+}$ -activated  $\text{K}^+$  channel showed negative slopes in a  $\text{K}^+/\text{Cs}^+$  solution (Draber and Hansen, 1994) or in  $\text{Na}^+$  (Weise and Gradmann, 2000). In the single-channel current of mammalian MaxiK, millimolar concentrations of cytosolic  $\text{Na}^+$  (Marty, 1983; Kahawara et al., 1990; DeCoursey et al., 1996) and  $\text{Ca}^{2+}$  (Cox et al., 1997) were shown to induce negative slopes.

To our knowledge, the functional role of the negative slope is unknown. Especially at positive potentials, the negative slope is found in a voltage range that would not occur in a living organism ( $>+100$  mV). Nevertheless, for the investigation of the biophysical principles of permeation and gating mechanisms in transport proteins, a clear description and understanding of the deviations from linear effects can provide important keystones.

In whole-cell experiments, the occurrence of negative slopes can easily be related to gating phenomena (Sakmann and Trube, 1984). In the case of single-channel recordings only a few investigations in *Chara* reached the temporal resolution to reveal fast gating as a cause of apparent current reduction (e.g., Klieber and Gradmann, 1993; Draber and Hansen, 1994). Revealing fast gating as the cause of the negative slope in human MaxiK was up to now impeded by insufficient temporal resolution. This limitation could be overcome by the approach of Schroeder and Hansen (2006) using filtering with a corner frequency of 50 kHz and an analysis based on  $\beta$  distributions (Fitz-Hugh, 1983; Yellen, 1984; Moss and Moczydlowski, 1996; Riessner, 1998; Schroeder et al., 2005) for the determination of the true single-channel current. The

benefit of such an approach is the assignment of saturation and gating effects to different functional units of the channel protein and the detection of interactions. The analysis leads to the hypothesis that fast gating at high positive potentials is caused by ion depletion in the cavity and/or the selectivity filter. Early hints to such a mechanism came from the effect of the permeant ion on gating (Almers and Armstrong, 1980).

## MATERIALS AND METHODS

### Electrophysiological Measurements

Patch clamp measurements were performed on inside-out patches of HEK293 cells, stably expressing a h-MaxiK  $\alpha$ -GFP construct and the  $\beta$ 1-subunit (Lu et al., 2006). The cells were a gift from U. Seydel and A. Schromm (Research Center Borstel, Borstel, Germany). Four different solutions were used symmetrically in the pipette and in the bath. They all contained 10 mM HEPES, pH was titrated with KOH to 7.2. The solutions named 50K, 150K, and 400K contained 50, 150, or 400 mM KCl, respectively, plus 2.5 mM  $\text{CaCl}_2$  and 2.5 mM  $\text{MgCl}_2$ . In some experiments,  $\text{NO}_3^-$  was used instead of  $\text{Cl}^-$ . This did not affect the channel properties (not depicted). In the solution named 150K-Mg/Ca, there was no  $\text{Ca}^{2+}$  and  $\text{Mg}^{2+}$  added. Instead 10 mM EDTA was given to chelate spurious divalent cations. Patch electrodes were made from borosilicate glass (Hilgenberg) coated internally with Sigmacote (Sigma-Aldrich), drawn on an L/M-3P-A puller (Heka) and had a resistance of  $\sim 25$  M $\Omega$  in 150 mM KCl. Tobias Huth introduced drying of the pipettes at 55°C overnight after pulling. This treatment increased seal probability and resistance up to 100 G $\Omega$  (not depicted). Single-channel currents under steady-state conditions were recorded by a Dagan 3900A amplifier (Dagan) with a 4-pole anti-aliasing filter (Besel) of 50 kHz. Data was stored on disc with a sampling rate of 200 kHz and analyzed with custom-made programs and Origin (see below). Liquid junction potential was not corrected, because it was  $<5$  mV in all experiments.

Baseline drift, membrane flickering, and other artifacts would distort the amplitude histograms and lead to wrong results in the  $\beta$  fit. Thus, all data had to be closely inspected and cleaned manually from sections showing these kinds of artifact by means of the software Kiel-Patch.

Apparent current amplitudes ( $I_{app}$ ) were determined by manually positioning horizontal lines within the current records (fit-by-eye) using the software Kiel-Patch. Riessner et al. (2002) have shown that this method is more reliable than fitting a sum of gaussians to the overall amplitude histogram. This and the following software is available at [www.zbm.uni-kiel.de/software](http://www.zbm.uni-kiel.de/software).

### Definitions

In a preceding paper (Hansen et al., 2003) we have defined true (or real) and apparent single-channel currents. In brief, the passage of ions through the filter is a stochastic sequence. We call the moment when a transition occurs  $t_n$ . Consider the distribution of the time intervals  $t_{n+1}-t_n$ . A state lasts from  $t_A$  to  $t_E$ , if the frequency of the time intervals in the range  $(t_A, t_E)$  can be described by an asymptotic stochastic function that is independent of the length of  $(t_A, t_E)$ . Usually,  $t_E-t_A$  is too short, and the asymptotic distribution is not reached. Then, assuming ergodicity, ensemble averaging over putative intervals with the same state from the same or additional records has to be employed.

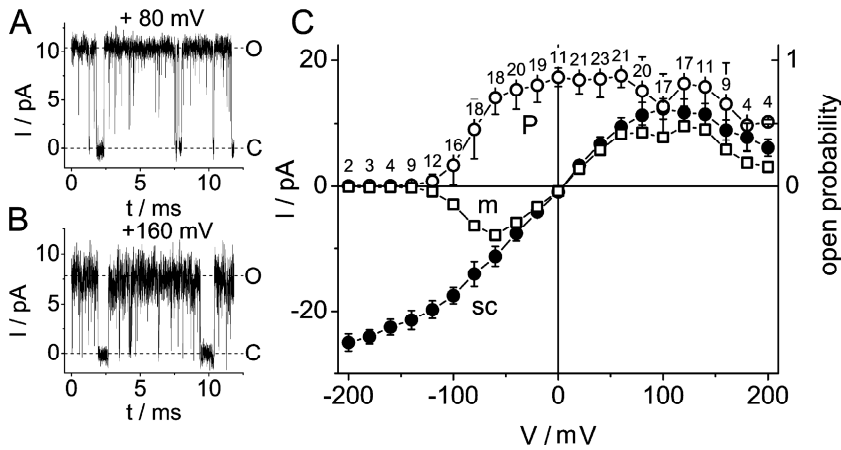


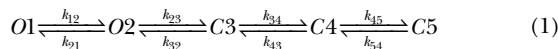
**Figure 1.** Correlation of single-channel current, open probability, and macroscopic current. (A and B) Representative sections of time series measured in 150 mM  $K^+$  and 2.5 mM  $Ca^{2+}$  and  $Mg^{2+}$  at (A) +80 mV and (B) +160 mV. Off-line averaging over 10 data points was used only for better display, not for analysis. The apparent single-channel currents are 10.4 and 7.8 pA, respectively. (C) Dependence of apparent single-channel current (sc, filled circles) and open probability (P, open circles) on membrane potential as obtained from inside-out patches with one to three channels in symmetric 150  $K^+$  solution. The “steady state macroscopic IV curve” (m, open squares) was reconstructed from the single-channel data by means of Eq. 4. The numbers of independent experiments are indicated for each voltage.

The true (or real) current  $I_{true}$  is the current average in the interval  $(t_A, t_E)$ . The apparent current  $I_{app}$  is the current average over a time interval that is assigned to an apparent state in an experimental record.  $I_{app}$  is identical to  $I_{true}$  if this interval is included in  $(t_A, t_E)$ .

#### Determination of the True Current Amplitude: $\beta$ Fit

The above definition of  $I_{true}$  is based on events that cannot be observed directly. Thus, analytical tools are required that can resolve the values of  $(t_A, t_E)$  and  $I_{true}$  from the single-channel patch clamp records even if  $(t_A, t_E)$  is shorter than the temporal resolution of the recording apparatus (fast gating), and  $I_{app}$  is smaller than  $I_{true}$ . Among the different tools for the evaluation of gating employed in our group, the analysis of  $\beta$  distributions (Schroeder et al., 2005) and of two-dimensional dwell-time distributions (Huth et al., 2007) turned out to be more efficient than one-dimensional dwell-time analysis (Blunck et al., 1998) or the direct fit of the time series (Albertsen and Hansen, 1994). Here, we use the approach of Schroeder and Hansen (2006) for the reconstruction of the true current by means of  $\beta$  distributions. Since there is no straightforward procedure to calculate  $\beta$  distributions obtained from higher-order filters (Riessner, 1998), simulations instead of deterministic algorithms were employed to provide the theoretical curves. This is quite time consuming during a fitting routine, but it turned out to be the most efficient way to resolve fast flickering.

In brief, the gating behavior of our data from the MaxiK channel can be described by a linear five-state model with two open and three closed states as shown below in Eq. 1 (Farokhi et al., 2000; Hansen et al., 2003).



However, for the determination of the true single-channel current it is not necessary to use the complete five-state model. If the flickering between the O states and C3 is so fast that averaging by the recording apparatus merges the output signal into one (apparent) current level, a truncated two-state model (Eq. 2) is sufficient for revealing the true current (Schroeder and Hansen, 2006).



The open-point histogram (distribution-per-level, Schroeder et al., 2004) of the apparent open state (excluding the long closed states) was obtained from the time series by means of an eight-order Hinkley detector included in the program Kiel-Patch (Schultze and Draber, 1993). For fitting the measured distribution per level ( $A_{exp,i}$ ) to that one obtained from times series simulated on the basis of the two-state Markov model ( $A_{theo,i}$ , Eq. 2), a Simplex algorithm (Caceci and Cacheris, 1984) was employed that minimizes

$$\text{error sum} = \sum_{i=1}^{N_I} \frac{(A_{exp,i} - A_{theo,i})^2}{A_{exp,i} + 0.1} \quad (3)$$

$N_I$  is the number of data points in the amplitude histograms (number of intervals on the current axis, in our case 4,096). The denominator prevents that the maximum values of the amplitude histogram get the highest statistical weight. The highest values are close to a gaussian distribution whereas the deviations carrying the information about fast gating are found at the slopes of the distribution. 0.1 is added in order to prevent overflow resulting from division by zero.

The fit algorithm (Schroeder and Hansen, 2006) also provides the automatic determination of the single-channel current  $I_{true}$ . However, here the current was used as a fixed parameter and changed stepwise in subsequent fits in order to study the dependence of the error sum on the assumed single-channel current (Fig. 3 B, below). The construction of this error sum curve was crucial to exclude fits that did not lead to a unique solution.

## RESULTS

### IV Curves in 150 mM $K^+$ with 2.5 mM $Ca^{2+}$ and $Mg^{2+}$ : Apparent Single-Channel and Steady-State Macroscopic Currents

Steady-state single-channel traces of hMaxiK  $\alpha + \beta 1$  of

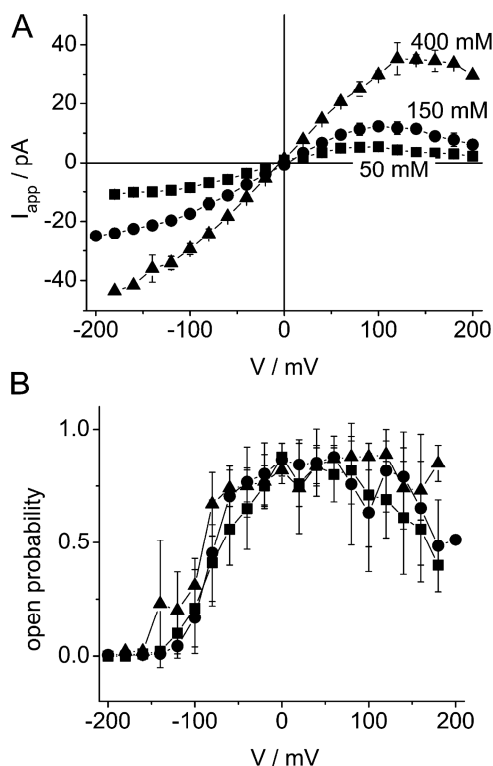


**Figure 2.** Influence of K<sup>+</sup> concentration on channel properties. (A) Apparent single-channel IV curves for low (50 mM, squares), standard (150 mM, circles), and high (400 mM, triangles) K<sup>+</sup> concentrations. (B) Voltage dependence of the open probabilities measured at 50, 150, and 400 mM K<sup>+</sup>. Measurements were done in symmetrical K<sup>+</sup> concentrations with 2.5 mM Ca<sup>2+</sup> and 2.5 mM Mg<sup>2+</sup> on either side. Data points present mean values from 1 to 23 experiments.

inside-out patches in symmetrical 150 K solution were recorded with a sampling frequency of 200 kHz and a 4-pole Bessel filter of 50 kHz. Fig. 1 (A and B) shows typical records obtained at +80 and +160 mV, respectively. The apparent single-channel current was obtained from a fit-by-eye as indicated by the horizontal lines and described above. Open probability (for slow gating) was determined by an eighth-order Hinkley detector.

In Fig. 1 C, the apparent single-channel current (closed circles) and the open probability (open circles) are shown. The channel is activated by positive membrane potential as known for MaxiK. The most striking feature of the single-channel IV curve is the negative slope at high positive voltages.

The occurrence of negative slopes has been reported more frequently from macroscopic MaxiK IV curves. In whole-cell recordings, negative slopes can occur on either side of the voltage range, at negative and at positive potentials (e.g., Cox et al., 1997). Gating of channel conductivity in different time domains influences single-channel and macroscopic currents in dif-

ferent ways. This is illustrated in Fig. 1 C. Steady-state macroscopic currents  $I_m$  were calculated from the product of single-channel current  $I_{SC}$ , the number  $n$  of channels in the cell and the open probability  $p$ :

$$I_m = I_{SC} \cdot n \cdot p \quad (4)$$

The resulting “macroscopic” IV curve (presented by the open squares in Fig. 1 C) is normalized to  $n = 1$  for the sake of comparison. This IV curve shows the typical features of macroscopic IV curves observed in the presence of high Ca<sup>2+</sup> concentrations (Cox et al., 1997), namely the occurrence of negative slopes in both voltage ranges. Even though the two negative slopes look quite similar, their origin is different. The negative slope of the macroscopic current at negative potentials is due to a decreasing open probability caused by slow (observable) gating. It does not originate from an effect on the single-channel current that shows saturation but no negative slope (curve sc in Fig. 1 C). In contrast, at high positive potentials (>+100 mV), the negative slope is mainly inherited from the apparent single-channel current.

In addition to the measurements in 150 mM K<sup>+</sup>, single-channel experiments were also done at 50 and 400 mM. In Fig. 2 A, the resulting IV curves are compared with that one in Fig. 1 C. The negative slope at positive membrane potentials occurs under all three conditions. However, the bending is shifted to higher positive membrane potentials with increasing K<sup>+</sup> concentration. A significant influence of K<sup>+</sup> concentration on the voltage dependence of the open probability cannot be verified (Fig. 2 B).

### True Single-Channel IV Curves

The comparison of the time series in Fig. 1 (A and B) with the IV curves in Fig. 1 C reveals that the negative slope of the apparent single-channel current at higher positive membrane voltages is accompanied by an increase in open-channel noise. The noise indicates that unresolved fast gating may hide the true current level (Hille, 1992; Hansen et al., 1997; Townsend and Horn, 1999). Thus, the effect of fast gating has to be eliminated in order to detect the true single-channel current. This is done by means of the  $\beta$  fit as described in Materials and Methods.

A typical example for this kind of analysis is illustrated in Fig. 3. From traces like those in Fig. 1 (A and B), amplitude histograms were generated (Fig. 3 A). The full amplitude histogram was split into distributions-per-level (Schroeder et al., 2004; Schroeder and Hansen, 2006) as presented in Fig. 3 A by the curves labeled O and C. The O-level distribution was fitted by the two-state model of Eq. 2 with the assumed single-channel current  $I_{fu}$  as a constant parameter. In Fig. 3

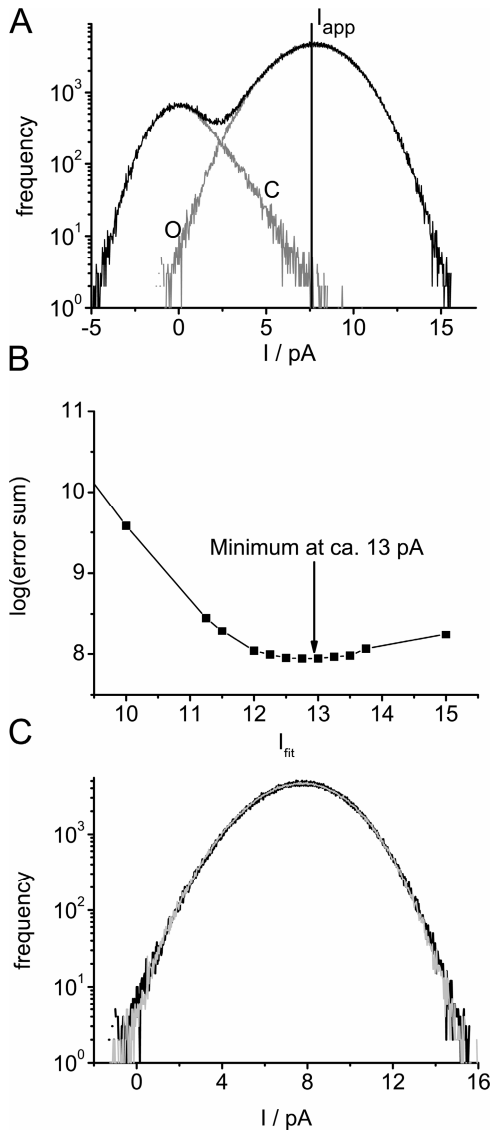


**Figure 3.** Example for the analysis of a single-channel time series, recorded at +160 mV in 150 K<sup>+</sup> (see Materials and Methods) on both sides of the membrane. (A) Full amplitude histogram (black) and distributions-per-level (gray). The apparent current  $I_{app}$  was 7.6 pA. (B) Dependence of the error sum on the putative single-channel current ( $I_{fit}$ ). Beta fits determined the optimum pair of rate constants for the O-C model (Eq. 2) with different assumed single-channel currents  $I_{fit}$ , which are given at the abscissa. The best fit could be obtained with  $I_{fit} = 13$  pA. (C) Comparison of the measured O-distribution (the same as in A) and the simulated one obtained from the best fit in B. The coincidence is so good that the two curves are nearly indistinguishable.

B, the dependence of the error sum (Eq. 3) on the assumed single-channel current  $I_{fit}$  (as given on the abscissa) is plotted. The minimum is quite shallow (due to the logarithmic scale), but the best fit (minimum error sum) can clearly be obtained around 13 pA (arrow), resulting in a ratio  $R = I_{true}/I_{app} = 1.7$ . The

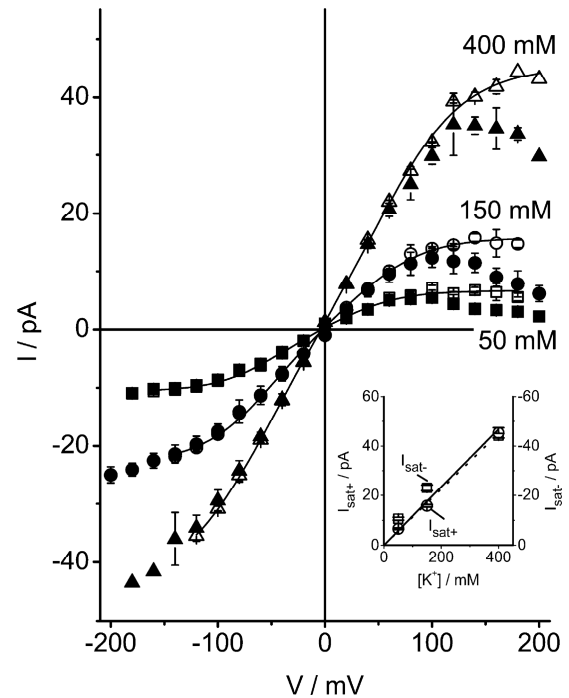


**Figure 4.** Apparent ( $I_{app}$ , closed symbols) and true ( $I_{true}$ , open symbols) single-channel IV curves for three different K<sup>+</sup> concentrations: 50 mM (squares), 150 mM (circles), and 400 mM (triangles). Solid lines: fit of  $I_{true}$  with Eq. 5, parameters are listed in Table I. Numbers of experiments are given in Figs. 2 and 6. Inset, concentration dependence of negative (squares and continuous line) and positive (circles and dotted line) saturation currents. Standard deviations are smaller than the size of the symbols. The straight lines present linear fits through the origin. The data are taken from Table I.

related approximation of the O-level distribution is very good, as shown in Fig. 3 C.

The analysis illustrated in Fig. 3 was applied to the data in Fig. 2 A for the whole voltage range. It resulted in corrected IV curves presenting the true single-channel current ( $I_{true} = I_{fit}$  at the minimum in Fig. 3 B). In Fig. 4, three pairs of IV curves are shown. Each pair consists of the apparent single-channel current (closed symbols) as already presented in Fig. 2 A, and the true single-channel current (presented by the open symbols). It has to be mentioned that the IV relationship of the true single-channel current  $I_{true}$  is asymmetrical; saturation at positive voltages leads to smaller currents than at negative voltages (see also Table I).

#### Saturation Currents

To get a more reliable determination of the saturation currents of the true single-channel current in Fig. 4, the IV curves were fitted by means of Eq. 5.

TABLE I

Summary of the Parameters Obtained from the Analysis of the True IV Curves and of the Gating Factors

	$g_{slope}^a$ / pS	$I_{sat+}^b$ / pA ( $=F\kappa_{oi}$ )	$I_{sat-}^b$ / pA ( $=-F\kappa_{io}$ )	$Fk_{oi,0}^b$	$k_{io,0}/k_{oi,0}^b$	$V_s^b$ / mV	$V_G^c$ / mV	$1/R_K^c$ ( $V_G = 60$ mV)
50 mM	$91 \pm 5$	$6.6 \pm 0.3$	$-10.6 \pm 0.6$	$3.2 \pm 2$	$2.0 \pm 0.4$	$29 \pm 9$	$60$ ( $51 \pm 7$ )	$15 \pm 0.9$
150 mM	$176 \pm 3$	$15.8 \pm 0.5$	$-23.0 \pm 1.2$	$7.1 \pm 2.5$	$1.7 \pm 0.2$	$33 \pm 6$	$60$ ( $57 \pm 3$ )	$25 \pm 0.7$
400 mM	$330 \pm 2$	$45.3 \pm 2.1$	$-44.2 \pm 0.9$	$16.5 \pm 2.3$	$1.2 \pm 0.1$	$39 \pm 4$	$60$ ( $62 \pm 5$ )	$63 \pm 2.3$

$R_K$  was determined with  $V_G$  fixed at 60 mV. Fit results for  $V_G$  as a free parameter are given in brackets. For fitting, averaged data were used, and the errors were estimated from the variance-covariance matrix as provided by the fitting routine in Origin.

<sup>a</sup> $g_{slopes}$  slope conductance was determined by a linear fit of the IV curves in the voltage range  $\pm 60$  mV.

<sup>b</sup> $I_{sat+/-}$ ,  $k_{oi,0}$ ,  $k_{io,0}/k_{oi,0}$ ,  $V_s$ , parameters of the true IV curves ( $I_{true}$ ; Fig. 4; Eq. 5).

<sup>c</sup> $V_G$ ,  $R_K$ , parameters of the gating factor (Fig. 6; Eq. 7).

$$I_{true} = F \frac{\kappa_{oi} \cdot k_{io,0} \cdot \exp\left(\frac{V}{V_s}\right) - \kappa_{io} \cdot k_{oi,0} \cdot \exp\left(-\frac{V}{V_s}\right)}{k_{io,0} \cdot \exp\left(\frac{V}{V_s}\right) + k_{oi,0} \cdot \exp\left(-\frac{V}{V_s}\right) + \kappa_{oi} + \kappa_{io}} \quad (5)$$

Eq. 5 is identical to the equation derived for the enzyme kinetic model of ion transport (Hansen et al., 1981; Hansen, 1986) with  $k_{io,0}$ ,  $k_{oi,0}$  being the scaling factors of the outward and inward voltage-dependent translocation steps, respectively, and  $\kappa_{oi}$  and  $\kappa_{io}$  including the binding of the ion on the cytosolic and on the luminal side, respectively. Because of the absence of an accepted transport model,  $V_s$ , the characteristic voltage of ion translocation, is just a phenomenological parameter. In simple models, it is related to the temperature potential  $u_T = kT/e = 26$  mV and the relative location of the energy barriers in the translocation path (Hansen et al., 1981).  $F$ ,  $V$ ,  $T$ ,  $k$ , and  $e$  have their usual meanings. This cyclic model is evident for cotransporters (Abramson et al., 2003; Huang et al., 2003), but was also found suitable for ion channels (Fisahn et al., 1986; Gradmann et al., 1987; Hansen and Fisahn, 1987), probably because of the cyclic scheme of site occupation as suggested by Morais-Cabral et al. (2001) or Bernèche and Roux (2005). Inspecting the mathematics behind different approaches shows that the crucial features of Eq. 5 also apply to other models including the law of mass conservation (probability normalization criterion) for the states in the filter (like that one of Nelson, 2002, based on a concerted single-file motion, Khalili-Araghi et al., 2006) or just voltage-independent loading reactions as in the simple four-compartment model in Fig. 8, below. The real biophysical background is of minor importance for the investigations here. It will be examined in a subsequent paper on a broader experimental basis.

The saturation currents are obtained for  $V$  approaching  $-\infty$  or  $+\infty$ :

$$I_{sat-} = -F\kappa_{io} \quad \text{and} \quad I_{sat+} = F\kappa_{oi}. \quad (6a \text{ and } 6b)$$

The curves resulting from the fits of the averaged data are shown in Fig. 4 as solid lines, and the parameters are given in Table I.

Fig. 4 and Table I show that saturation currents are asymmetrical for the two lower potassium concentrations. The loading reactions on either side of the selectivity filter have at least two major components: diffusion limitation and exchange of the water shell for the carbonyl groups of the filter. The asymmetry is stronger for low potassium concentrations, indicating

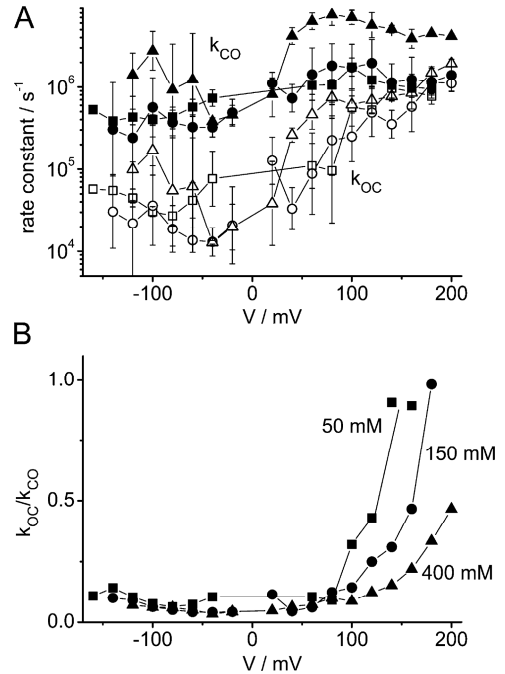


**Figure 5.** Rate constants for the reduced two-state Markov model (Eq. 2). Squares, 50 mM K<sup>+</sup>; circles, 150 mM K<sup>+</sup>; triangles, 400 mM K<sup>+</sup>. (A) Absolute values of the open-closed ( $k_{oc}$ , open symbols) and the closed-open transitions ( $k_{co}$ , closed symbols). (B) Ratio of  $k_{oc}$  and  $k_{co}$  as calculated from the data in A. Numbers of experiments are given in Fig. 6.

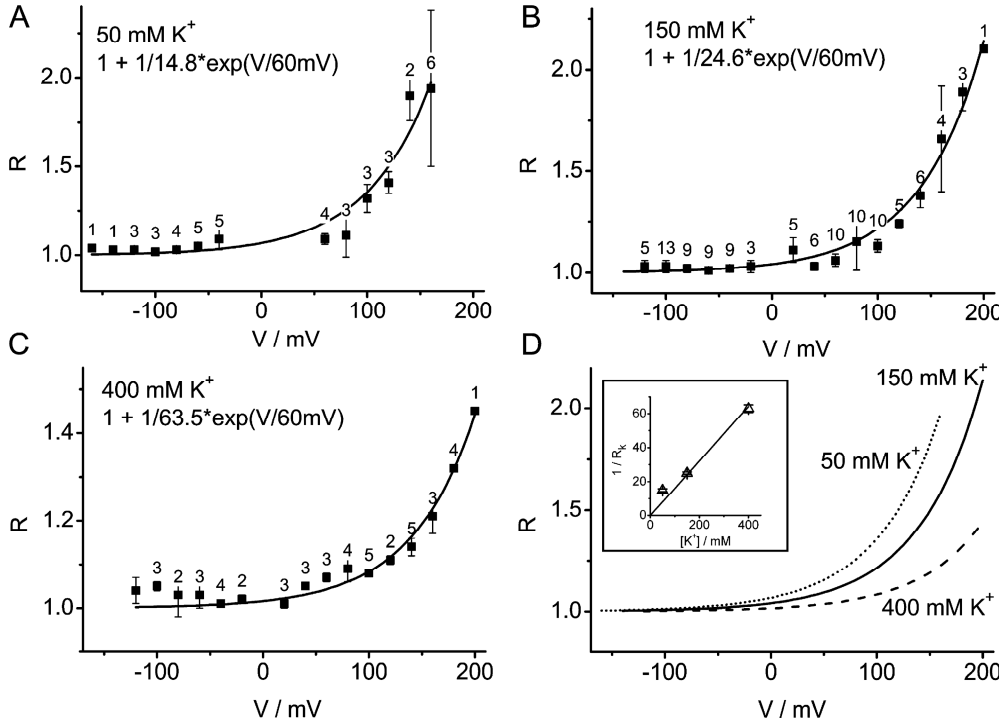


**Figure 6.** Fit (smooth lines, with fixed  $V_G = 60$  mV) of the current reduction  $R$  ( $I_{true}/I_{app}$  in Fig. 4) for three  $K^+$  concentrations by means of Eq. 7: (A) 50 mM, (B) 150 mM, (C) 400 mM. The parameters of the fits are given in the graphs and in Table I. (D) Comparison of the fitted curves in A–C. Numbers of individual experiments are given at the curves. Inset, concentration dependence of the amplitude factor  $1/R_K$ . Standard deviations are smaller than the size of the symbol. The straight line is a linear fit through the origin. The data are taken from Table I.

that the entry from the cytosolic side has a stronger diffusional component. This is in line with the results of Brelidze and Magleby (2005) that diffusion limitation induced by sugars can be overcome by high  $K^+$  concentrations in the cytosol.

#### Rate Constants of Flickering

The fits of the  $\beta$  distributions (Fig. 3) do not only deliver the true single-channel current (as illustrated in Fig. 3 B), but also a related pair  $k_{OC}$  and  $k_{CO}$  of rate constants (Eq. 2; Fig. 5 A), roughly corresponding to  $k_{23}$  and  $k_{32}$  in Eq. 1. In a previous paper (Schroeder and Hansen, 2006), we have shown that the usage of a truncated model after the processing of the data through the Hinkley detector (as described in Materials and Methods) leaves the true single-channel current unaffected. However, this method can impose small errors on the determination of the rate constants. Nevertheless, the following statements would also be obtained from a more refined (five-state model) analysis. (a) The dominant voltage dependence can be attributed to  $k_{OC}$ . The increase of  $k_{OC}$  at positive voltages leads to shorter open-dwell times and thus to a decrease of the apparent (averaged) single-channel current. (b) The high scatter impedes the detection of small effects of the ion concentration on the rate constants. (c) The determination of the ratio of the rate constants (Fig. 5 B) is much more reliable than that of the absolute values, thus making the influence of concentration obvious, which is scarcely detectable in Fig. 5 A.

#### Model-based Analysis: Mechanisms of Current Reduction

The current reduction by fast gating, i.e., the ratio of  $I_{true}$  and  $I_{app}$  in Fig. 4, was analyzed with the model described in the Appendix. It is based on the assumption that ion depletion in the cavity/selectivity filter causes the filter to flicker. This model predicts that the voltage dependence of the gating factor  $R = I_{true}/I_{app}$  is a simple exponential function of the membrane voltage  $V$ :

$$R = \frac{I_{true}}{I_{app}} = 1 + R_K \exp\left(\frac{V_0}{V_G}\right). \quad (7)$$

Indeed, Fig. 6 (A–C) shows that the data can neatly be fitted by Eq. 7. Fig. 6 D presents a comparison of the three fitted curves in A–C. The resulting parameters are given in Table I.

Fitting the  $R$  curves in Fig. 6 resulted in  $V_G = 51, 57,$  and  $62$  mV for 50, 150, and 400 mM  $K^+$ , respectively (in brackets in Table I). The low signal-to-noise ratio found in 50 mM  $K^+$  decreased the reliability of the data (Fig. 6 A). To get comparable estimates of the factor  $1/R_K$ , all  $R$  curves were fitted additionally with a fixed  $V_G$  of 60 mV (average of the values at 150 and 400 mM  $K^+$ ).

#### Independence on $Ca^{2+}/Mg^{2+}$

It has often been reported that  $Ca^{2+}$  and  $Mg^{2+}$  not only activate MaxiK channels but also block at millimolar

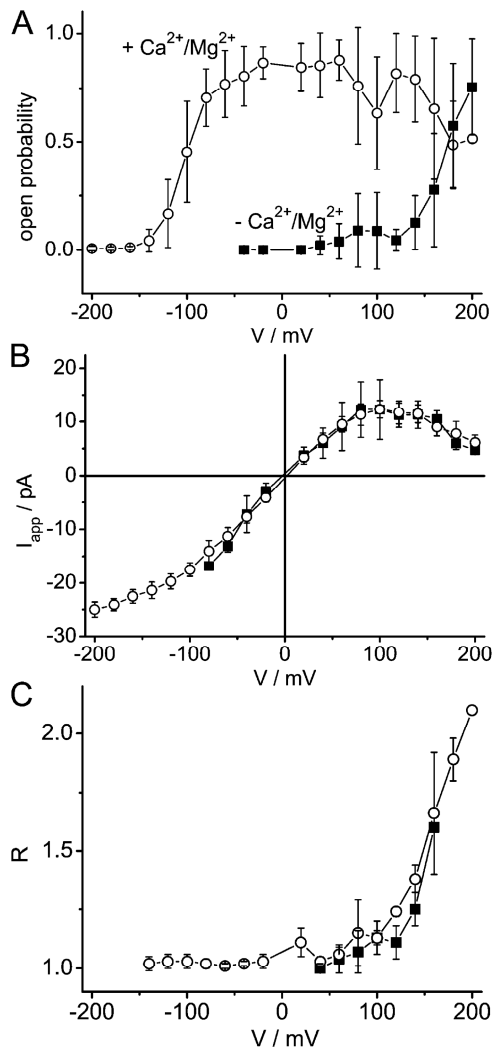


**Figure 7.** Effect of divalent cations. Open circles present data obtained from solutions with divalent cations (150K), closed squares those without divalent cations (150K-Mg/Ca). (A) The open probability of the channel is strongly reduced without divalent cations. (B) The negative slope of the single-channel current is independent of Ca<sup>2+</sup> and Mg<sup>2+</sup>. (C) Also the ratio of true and apparent current ( $R$ , Eq. 7) is not influenced. Data with divalent cations are taken from Figs. 1 and 6. There are three to nine experiments without divalent cations per data point in A and B and one to five in C.

concentrations (e.g., Ferguson, 1991; Bertl et al., 1993; Cox et al., 1997). To rule out this effect, measurements were performed under 0 Ca<sup>2+</sup>/Mg<sup>2+</sup> conditions (with 10 mM EDTA, solution 150K-Mg/Ca) and compared with those done under saturating concentrations of the two divalent ions (2.5 mM each, solution 150K). The well-known influence on open probability was observed (Fig. 7 A), but there was no significant effect on the single-channel IV curves (Fig. 7 B). The analysis with  $\beta$  fits also shows that the current reduction caused by fast flickering stays the same with and without diva-

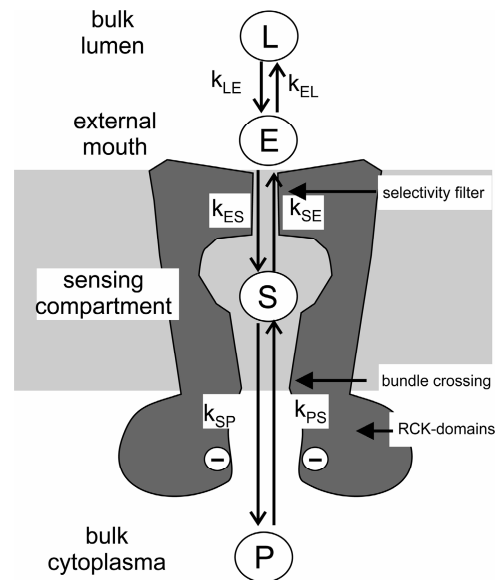


**Figure 8.** Model for ion movement between bulk cytoplasm ( $P$ ), the “sensing compartment” ( $S$ , cavity and/or selectivity filter), the external vestibule ( $E$ ), and the bulk lumen ( $L$ ). The rate constants on the arrows are those employed in the calculations in the Appendix.

lent cations (Fig. 7 C). Thus, we can rule out that the negative slope at positive potentials results from a Ca<sup>2+</sup> or Mg<sup>2+</sup> block. This corresponds to the findings of Cox et al. (1997), who reported a slight, [Ca]<sub>i</sub>-independent negative slope in MaxiK channels at internal Ca<sup>2+</sup> concentrations <124  $\mu$ M. This is similar to the findings of Bertl et al. (1993) that rate constants related to the closed state of the Ca<sup>2+</sup>-activated K<sup>+</sup> channel in *Saccharomyces cerevisiae* (probably a MaxiK), which cause flickering in the submillisecond range, are not sensitive to Ca<sup>2+</sup>, in contrast to the rate constants of the other two closed states with slower gating. This was also observed for fast gating in MthK (Li et al., 2007). The independence on a blocking ion is a crucial feature for the model created from the analysis of the data.

## DISCUSSION

### Reliability of the Separation of Gating and Permeation Effects

The results in Figs. 4 and 6 stress the importance of high temporal resolution for the distinction of the effects resulting from gating and permeation (Moss and Moczydlowski, 1996; Hansen et al., 1997, 2003; Townsend and Horn, 1999; Farokhi et al., 2000). After elimination of the gating effect in the apparent open-channel current, the IV curve of single-channel current shows saturation at high positive membrane potentials. The negative slope is eliminated.

The definition of  $I_{true}$  (see Materials and Methods) is still outside the reach of present experimental tools. Thus, it has to also be asked whether the saturation effect of what is called true single-channel current at high positive and negative potentials (Fig. 4) might originate from even faster gating processes that cannot be resolved in the experiments reported here. At very high gating frequencies,  $\beta$  distributions become gaussian and narrow again (Central Limit Theorem; Feller, 1968; Fig. 4 in Schroeder and Hansen, 2006). The temporal resolution obtained by the experiments above reached  $\sim 0.5 \mu\text{s}$ . This has to be compared with the average time required for a passage of a single ion that is 10 ns for a current of 16 pA. Thus, there is an average number of 50 ions passing the channel in 500 ns. There is not much numerical freedom for the introduction of additional undetected fast gating effects if the concept of classical Markov modeling is employed. If assumed gating frequencies come into the range of the average time between the transitions of two ions, gating and permeation mechanisms can no longer be separated. Since this kind of effect cannot be verified experimentally, and since there are reasonable biophysical mechanisms (discussed below) leading to saturation, it is assumed here that permeation effects and gating effects are clearly separated in the data of Fig. 4.

#### A Mechanism Correlating Saturation and Gating

A key for revealing the mechanism causing fast gating may be found in the observation that reduction of the true current by saturation (permeation effect) and by flickering (gating effect) occur (more or less) concomitantly (Fig. 4). In Fig. 8, the sensing compartment  $S$  plays the crucial role.  $S$  may be assigned to the cavity and/or the selectivity filter. If assigned to the cavity, a binding site may be assumed. For instance, Lu et al. (2001a) suggested that C169 binds  $\text{Ti}^+$  in Kir2.1. Alternatively, the protein backbone may feel the coordination forces for the ion in the cavity. Here, we prefer a crucial role of the selectivity filter, keeping in mind that a role of the cavity cannot be excluded.

With increasing positive membrane potential, the rate constant  $k_{SL}$  (comprising  $k_{SE}$  and  $k_{EL}$ ) of emptying the compartment  $S$  (Eq. A3; Fig. 8) exceeds the rate constant  $k_{PS}$  of refilling. This results in a depletion of ions in the cavity and/or the selectivity filter. The depletion leads to an instability of the selectivity filter and causes fast flickering as described by the gating factor  $R$  in Fig. 6. Three features of the model of Fig. 8 described in quantitative terms in the Appendix have to be mentioned. (1) ‘‘Ion concentration’’ in the cavity/filter has to be replaced by the average dwell time of probably about four ions in the cavity and filter. (2) The ion concentration does not exert a direct effect

but a parametric effect. A direct effect would imply that the efflux to the lumen decreases the ion concentration in  $S$  until the filter shuts. It would reopen when refilling from the cytosol has restored the ion concentration. Such a direct effect does not lead to dwell times in the microsecond range, because the reservoir  $S$  containing only a few ions would be filled up in the 10-ns range. The essential feature of the parametric effect is that the rearrangement of the protein backbone has a time constant that leads to integration over several periods of ion depletion during the open states of the flickering selectivity filter. The resulting conformational changes modulate the open/close ratio of the fast gating. (3) This parametric effect keeps the ion concentration at an average value that prevents the complete collapse of the filter.

Fitting the  $R$ -factor in Fig. 6 with Eq. A9 leads to plausible results, i.e., the exponential increase of  $R$  with membrane potential making obvious that the exponentially increasing (Eq. A5) rate constant of ion transfer in the selectivity filter results from a typical voltage-driven ion transfer mechanism (Lauger and Stark, 1970; Hansen et al., 1981; Hansen, 1986). However, the comparison with the fits of the IV curves in Fig. 4 by means of Eq. 5 reveals a discrepancy; the characteristic voltage  $V_G = 60 \text{ mV}$  (gating, Eq. A9) is higher than the characteristic voltage  $V_S = 35 \text{ mV}$  (IV curve, Eq. 5). Both of them should be higher than  $u_T = 26 \text{ mV}$  (Hansen et al., 1981), but equal in the simplest form of the model in Fig. 8.

This discrepancy makes obvious that the mathematical description of this model in the Appendix needs further refinements. The most likely extension would start from the assumption that  $k_{SE}$  of the selectivity filter feels only the part  $bV$  of the full membrane potential  $V$  (leading to  $V_G = 26 \text{ mV}/b$ ), and that another part of the membrane potential influences the loading reaction  $k_{PS}$ . Then,  $k_{PS}$  would consist of a voltage-independent term (which determines the saturation current  $Fk_{PS}$ , e.g., exchanging the water shell for the channel environment) and a voltage-dependent component. The voltage-dependent part of  $k_{PS}$  (and its equivalent  $\kappa_{oi}$ ) exerts its influence in the numerator for the IV curves (Eq. 5), but in the  $R$ -factor both numerator and denominator would be voltage dependent (Eq. A8). This may explain why  $V_G$  is higher than  $V_S$ .

There are still other mechanisms feasible leading to different  $V_S$  and  $V_G$ . Thus, it does not make sense to implement a more sophisticated version of  $k_{PS}$  ( $\kappa_{oi}$ ) in Eq. 5 and in the Appendix, because the present experimental findings do not provide any means to distinguish models. The basic message is that a voltage drop over the loading reaction  $k_{PS}$  is a likely explanation for the difference between  $V_S$  and  $V_G$ .

A similar problem is found in the comparison of the

concentration dependence of the saturation currents (Table I; Fig. 4, inset) and  $1/R_K$  resulting from the gating analysis (Table I; Fig. 6, inset). In either case, a linear relationship to  $[K^+]_p$  would be expected for a simple model, whereas a Michaelis-Menton-like dependence is predicted by the models including a probability normalization criterion (Hansen et al., 1981; Fisahn et al., 1986; Hansen 1986). Linearity roughly holds for the saturation currents, but it is weaker for  $1/R_K$ . Also here, a more elaborated kinetic model would be premature as long as the real kinetic scheme and putative superimposed direct effects of  $K^+$  concentration and of voltage on channel structure are not supported by experimental findings.

#### Assumption 1: Gating by the Selectivity Filter

The crucial role of the selectivity filter in the model of Fig. 8 may be uncommon in the light of the majority of investigations where the inner gate (Perozo et al., 1999; Loussouarn et al., 2000) or the ball and chain mechanism (Catterall, 2000; Bentrop et al., 2001) are the preferred candidates. In the MaxiK channel, the S0 helix brings the N terminus to the luminal side. This eliminates inactivation by the ball-and-chain mechanism (Koval et al., 2007) and makes the MaxiK a favorite object of patch clamp analysis. Thus, the decision has to be made between inner gate and selectivity filter in MaxiK.

Fluorescence studies revealed that gating probably arising from the selectivity filter became apparent when the inner gate was open (Blunck et al., 2006). The involvement of the selectivity filter in gating gets strong support from concomitant changes in ion selectivity (Zheng and Sigworth, 1997; Kiss et al., 1999). The question of whether fast gating originates from the selectivity filter or inner gate finds ambiguous answers in the literature. It seems that both gates are capable of fast and slow gating. Some papers assign the fast gating to the inner gate and slower processes to the selectivity filter (Kir2.1, Lu et al., 2001a,b; Xie et al., 2004; Yeh et al., 2005; Fujiwara and Kubo, 2006; GIRKGIRK, Yi et al., 2001; KcsA, Cordero-Morales et al., 2006a,b). In some papers it is just the other way round (Kir 6.2, Trapp et al., 1998; Proks et al., 2001; Proks et al., 2005; MthK, Li et al., 2007; *Shaker*, Zheng et al., 2001). This discrepancy may be resolved by findings of Xie et al. (2004) indicating that in Kir2.1, fast gating can be mediated by either gate, depending on whether mutations are located near the GYG motif or in the cytosolic ring. In MaxiK channels, the relationship between slow gating and the inner gate was revealed in mutants with modified length of the linker between the inner gate and the cytosolic gating ring (Niu et al., 2004).

Whereas the studies mentioned above have demon-

strated that altering the channel's backbone changes the gating behavior (e.g., by disruption of salt bridges in the P-loop of IRK1 mutants; Yang et al., 1997), here an interaction between the ionic milieu and the protein is postulated. This is in line with many observations in earlier papers. Almers and Armstrong (1980) have observed in squid axons "that a  $K^+$  channel is normally occupied by one or more small cations, and becomes nonfunctional when these cations are removed." This so-called "foot-in-the-door effect" (Yeh and Armstrong, 1978) or "modulation of gating by a site inside the pore" (Matteson and Swenson, 1986) has been verified by a plethora of papers up to now in different kinds of channels (e.g.,  $K^+$  channel in squid, Swenson and Armstrong, 1981; delayed rectifier, Spruce et al., 1989; MaxiK, Demo and Yellen, 1992; *Shaker*, Melishchuk et al., 1998; KcsA, LeMasurier et al., 2001; *Shaker* and Shab, Ambriz-Rivas et al., 2005; Kv2.1, Immke et al., 1999; Wood and Korn, 2000; Kv1.5, Wang et al., 2000). Constriction of the filter is indicated by the conduction of  $Na^+$  in the absence of  $K^+$  (Immke et al., 1999).

Searching for a mechanism mediating the influence of the ionic milieu on filter stability, it is tempting to assume a mechanism related to the collapse of the selectivity filter of KcsA channels crystallized at very low  $K^+$  concentrations (3 mM; Zhou et al., 2001). This structure with flipped backbone carbonyl groups is similar to that predicted in molecular dynamics simulations of V127T mutations of Kir6.2 (Capener et al., 2003). Bernèche and Roux (2005) found in free energy molecular dynamics simulations of the filter of KcsA that the occupation of the  $S_2$  position by a  $K^+$  ion is important for preventing the  $180^\circ$  turn of a single V76-G77 amide plane followed by reorientation of T75-V76. Relaxation from this stable nonconducting state of broken symmetry is expected to be in the range of 0.1 ms, far too slow for the events observed here. It may be tempting to assign the fast flickering at positive membrane potentials to the reversible reorientation of the V76-G77 amide plane. However, further experimental work is required to prove whether this or other mechanisms are the origin of the fast flickering. A snapshot of the postulated induction of flickering in dependence on ion concentration seems to have been found in KcsA crystals grown in  $Tl^+$  solutions around a midpoint concentration of 80 mM. The selectivity filter is poorly defined in these structures, but ion occupancy measurements show that about half the channels in the crystal are in the conductive and half in the collapsed state (Zhou and MacKinnon, 2003). However, to our knowledge, structural data from the filter in  $K^+$  concentrations in the critical range between 3 and 200 mM are not yet available, in contrast to ion distributions (Morais-Cabral et al., 2001).

The ion-induced structural rearrangements (Capener et al., 2003) related to fast gating of the selectivity filter seem to be different from those of slow C inactivation. In contrast to C inactivation, there is no obvious relationship between flickering and selectivity as shown in molecular dynamics calculations (Khalili-Araghi et al., 2006) and in physiological studies on mutants of the GYG motif (Lu et al., 2001b).

For the data presented here, the above considerations would imply that  $k_{oc}$  and  $k_{co}$  in Fig. 5 A are the inverse dwell times in the conducting and in the collapsed state, respectively. Fast flickering as a consequence of a disturbed ionic milieu in the filter of MaxiK channels was also suggested by Piskorowski and Aldrich (2006) in the presence of  $Tl^+$ . Similar results were obtained in our group (unpublished data). A negative slope due to current reduction by flickering occurred at negative potentials when luminal  $Tl^+$  dilutes the  $K^+$  concentration in compartment *S* of Fig. 8 (not depicted). Nevertheless, Ambriz-Rivas et al. (2005) pointed out that different  $K^+$  channels may behave differently with respect to  $K^+$  depletion and presence of  $Na^+$ .

There are still open questions like that of irreversibility. Almers and Armstrong (1980) found that the depletion of ions caused irreversible loss of conductivity. It may be imagined that once  $K^+$  is excluded from the filter, the collapsed structure prevents reentering and opening. Two aspects of the model in Fig. 8 may prevent this. First, the hypothesis neglected above may gain importance, namely, that the sensor for  $K^+$  depletion is not in the filter, but in the cavity. It may control the exit of ions from the filter and thus prevent the collapse, but also the transport. Such an imprisoning of the ion under depletion may provide an explanation for the findings of Baukowitz and Yellen (1996) that the exit rate of the last ion from the  $K^+$  channel was 100 times lower than the normal transfer rate. Alternatively, the final collapse of the filter may be related to structural rearrangements with time constants longer than those of flickering. Then flickering would prevent that the average ion concentrations in the cavity and in the filter would fall below a critical value. Furthermore, the above model may lead to the question of whether this flickering does also occur when bundle crossing prevents the delivery of ions from the cytosol. Answering these questions is still beyond the scope of present experimental approaches.

#### Assumption 2: Voltage-independent Rate Limitation

As mentioned above, rate limitation by  $k_{ps}$  in Fig. 8 may have two components: (1) exchange of the water shell for the channel environment and (2) diffusion limitation. Even though the channel mimics the water shell quite well, the transition is probably not absolutely

smooth, and thus may create a rate-limiting energy barrier.

One component of diffusion limitation arises from the capture radius at the entrance of the channel. In gramicidin channels, this was found to be more important for rate limitation than dehydration (Andersen and Feldberg, 1996). Surface charges as occurring in  $K^+$  channels can enrich the ions near the channel entrance (Green and Andersen, 1991) and thus weaken diffusion limitation. Indeed, channels with high conductance carry negative charges at the cytosolic end of the inner helix (Kcv, Tayefeh et al., 2007), and these charges clearly determine the saturation current (BK, Brelidze et al., 2003; BK and MthK, Nimigeon et al., 2003). They are absent in low-conductance channels like Kir2.1. Nevertheless, also here the negative charges in the more distant hanging gondola contribute to the enhancement of current (Xie et al., 2004; Yeh et al., 2005; Fujiwara and Kubo, 2006). Diffusion limitation at the luminal side seems to be less severe. Nevertheless, neutralizing the luminal negative charges in a mutant of Kir2.1 (Alagem et al., 2001; Murata et al., 2002) decreases inward current.

A more direct approach to the effect of diffusion limitation seems to be provided by experiments with sugars on the cytosolic side (Brelidze and Magleby, 2005). Sugars putatively hinder diffusion and result in a decrease of outward saturation current of MaxiK channels as would be predicted by the model in Fig. 8. However, in the data of Brelidze and Magleby (2005) there are no signs of stronger flickering. Preliminary experiments in a student's course (unpublished data) have revealed that the voltage dependence of the factor *R* in Fig. 6 B was not influenced when 400 mM sucrose decreased the saturation current.

These experiments seem to be in contradiction to the predictions of the model in Fig. 8. Even though the model explains the effect of different cytosolic  $K^+$  concentrations (Fig. 6) quite well, the necessity to incorporate additional effects, e.g., direct interaction of sugar and channel structure, cannot be denied. Roux (2006) commenting on the results of Ahern et al. (2006) stated that the discrepancy between physiological findings and molecular dynamics simulations on one side and structural data on the other side in the case of TEA binding from the external side may be "the tip of a large iceberg of surprises and misconceptions" about the structure of the pore. Thus, apparently inconsistent results should be interpreted with care as long as more precise results are not available.

#### Conclusions

The crucial assumption of the model in Fig. 8 that ion depletion in the selectivity filter causes flickering explains the data of the present investigation quite con-

vincingly and in addition is supported by many observations dealing with the effect of the permeant ion on gating and filter stability. However, in experiments that artificially establish rate limitation on the cytosolic side, flickering is not induced. This indicates that the model in the Appendix is still an oversimplification (for the sake of analytical tractability) and additional effects have to be incorporated like direct action of potential and solutes on the filter structure. Nevertheless, it yields a stimulus to reconsider many experimental findings, e.g., those dealing with binding sites near or inside the filter. Eliminating an effect by a mutation does not necessarily mean that a binding site has been eliminated. Instead, it has to be taken into account that a protein is a quivering mechanical device. Mutations at one place may change the geometrical conditions for ion–filter interaction along the whole filter length and modify ion–filter interaction at a quite distant location.

## APPENDIX

### A Model Describing the Putative Influence of Ion Concentration in S (Cavity/Filter) on Fast Gating

The model of Fig. 8 is employed for a quantitative evaluation of fast gating. The compartments are the cytoplasm (index  $P$ ) and the lumen (index  $L$ ), both representing the bulk phases on either side of the channel, and two intermediate compartments (indices  $S$  and  $E$ ).  $E$  is the external vestibule of the channel, and  $S$  is called the sensing compartment, because the stability of the protein, and thus the rate constants of flickering, depends on the ion concentration in this compartment as described in the Discussion. In our calculations, this sensing compartment ( $S$  in Fig. 8) can be the cavity and/or the selectivity filter.

In a simple model, with voltage-independent loading ( $k_{PS}$ ,  $k_{LE}$ ) and discharge reactions ( $k_{SP}$ ,  $k_{EL}$ ) on either side and voltage-sensitive translocation through the selectivity filter ( $k_{SE}$ ,  $k_{ES}$ ), the current is

$$I_{true} = F \frac{k_{PS} k_{SE} k_{EL} [K^+]_P - k_{LE} k_{ES} k_{SP} [K^+]_L}{k_{SE} k_{EL} + k_{SP} k_{EL} + k_{SP} k_{ES}}, \quad (\text{A1})$$

with  $F$  being the Faraday constant. At extreme voltages, the currents saturate and take the constant values

$$I_{sat+} = I_{true} (V \rightarrow +\infty) = F \kappa_{oi} = F k_{PS} \cdot [K^+]_P \quad (\text{A2a})$$

(A2B)

$$I_{sat-} = I_{true} (V \rightarrow -\infty) = -F \kappa_{oi} = -F k_{LE} \cdot [K^+]_L,$$

with  $\kappa_{io}$  and  $\kappa_{oi}$  being the voltage-independent loading reactions of Eq. 5 (Hansen et al., 1981; Hansen, 1986) and  $k_{PS}$  and  $k_{LE}$  the loading rate constants for  $[K^+]_{P,L} = 1$  mM.

The ion concentration in the sensing compartment during the open state of the filter can be calculated from the balance of influx from the cytosol ( $k_{PS}$ ) and efflux to the lumen ( $k_{SL}$ ). Because of the low capacity of  $S$  (maximum three ions in the filter, one in the cavity; Zhou and MacKinnon, 2003; Compoin et al., 2004) and the resulting very fast equilibration, steady-state conditions can be assumed leading to

$$[K^+]_S = \frac{k_{PS}[K^+]_P + k_{LS}[K^+]_L}{k_{SP} + k_{SL}}, \quad (\text{A3})$$

with  $k_{SE}$ ,  $k_{EL}$  being represented by the gross reaction  $k_{SL}$ . At high positive voltages, backflow from the lumen can be ignored, and  $k_{SE} \gg$  all others. This results in the approximation

$$[K^+]_S = \frac{k_{PS}[K^+]_P}{k_{SL}} = \frac{k_{PS}[K^+]_P}{k_{SE} \frac{k_{EL}}{k_{LE}}}. \quad (\text{A4})$$

It has to be mentioned that ion concentration means average dwell time of ions in  $S$ . During the closed time of the filter, equilibrating with the cytosol leads to a recovery of the concentration in  $S$ . At high positive potentials, outward current is determined by the entry reaction from the cytosol into the (Eq. A2a). However, in contrast to the constant current, the concentration  $[K^+]_S$  decreases with increasing  $k_{SE}$  in the numerator of Eq. A4. This leads to flickering according to the findings of crystal structure analysis (Zhou et al., 2001; Zhou and MacKinnon, 2003) and molecular dynamics simulations (Compoin et al., 2004). The presence of ions in  $S$  is required for structural stability probably in order to compensate electrostatic forces (Zhou and MacKinnon, 2003). The role of  $K^+$  for stabilizing the tetrameric filter structure also became obvious from the demand of permeant ions for protecting the oligomer of Kcv from dissociation upon heating (Pagliuca et al., 2007).

To set up a quantitative description of the effect on gating behavior we have to make two assumptions. (1) For the voltage dependence of  $k_{SL}$  we assume that the ions have to jump over at least one energy barrier (in the selectivity filter), resulting in

$$k_{SL} = k_{SL,0} \exp\left(\frac{V}{V_G}\right). \quad (\text{A5})$$

(2) For the relationship between gating and  $[K^+]_s$ , a very simple approach is chosen:

$$k_{OC} = k_{OC,1} [K^+]_s^{-1}, \quad (\text{A6})$$

implying that the open–closed transitions become faster with decreasing  $[K^+]_s$ . This probably is an oversimplification. However, considering alternative approaches including averaging over closed and open times of the filter showed that already this simple version can create an understanding of the basic processes. A higher sophistication would become detached from the available experimental background.

Fig. 5 A indicates that  $k_{CO}$  is not significantly dependent on membrane potential (or concentration in  $S$  of Fig. 8). This implies that the relaxation from the closed state is quite independent of the distorting parameter (compare Fig. 5 B). When the rate constants of gating  $k_{CO}$  and  $k_{OC}$  are faster than the filter frequency, the apparent current is proportional to the open probability:

$$I_{app} = \frac{k_{CO}}{k_{CO} + k_{OC}} I_{true}. \quad (\text{A7})$$

Inserting Eqs. A6, A4a, and A5 into Eq. A7 leads to

$$\frac{I_{app}}{I_{true}} = \frac{k_{PS}[K^+]_P k_{CO}}{k_{SL,0} \exp\left(\frac{V}{V_G}\right) k_{OC,1} + k_{PS}[K^+]_P k_{CO}}, \quad (\text{A8})$$

with  $k_{SL,0}$  being  $k_{SL}$  at 0 mV. Eq. A8 is a Boltzmann-type equation. The inverse relationship can be fitted by an exponential

(A9A AND A9B)

$$R := \frac{I_{true}}{I_{app}} = 1 + R_K \exp\left(\frac{V}{V_G}\right) \text{ with } R_K = \frac{k_{OC,1} k_{SL,0}}{k_{CO} k_{PS} [K^+]_P}.$$

We are grateful to Imke Diddens for doing some of the patch clamp experiments and to Sonja Vollbehre for taking care of the HEK cells.

This work was supported by the Deutsche Forschungsgemeinschaft Ha712/14-1,2.

Olaf S. Andersen served as editor.

Submitted: 13 April 2007

Accepted: 7 June 2007

## REFERENCES

Abramson, J., I. Smirnova, V. Kasho, G. Verner, H.R. Kaback, and S. Iwata. 2003. Structure and mechanism of the lactose permease of *Escherichia coli*. *Science*. 301:610–615.

Ahern, C.A., A.L. Eastwood, H.A. Lester, D.A. Dougherty, and R. Horn. 2006. A cation- $\pi$  interaction between extracellular TEA and an aromatic residue in potassium channels. *J. Gen. Physiol.* 128:649–657.

Alagem, N., M. Dvir, and E. Reveny. 2001. Mechanism of  $Ba^{2+}$  block of a mouse inwardly rectifying  $K^+$  channel: differential contribution by two discrete residues. *J. Physiol.* 534.2:381–393.

Albertsen, A., and U.P. Hansen. 1994. Estimation of kinetic rate constants from multi-channel recordings by a direct fit of the time series. *Biophys. J.* 67:1393–1403.

Almers, W., and C.M. Armstrong. 1980. Survival of  $K^+$  permeability and gating currents in squid axons perfused with  $K^+$ -free media. *J. Gen. Physiol.* 75:61–78.

Ambriz-Rivas, M., L.D. Islas, and F. Gomez-Lagunas. 2005.  $K^+$ -dependent stability and ion conduction of Shab  $K^+$  channels: a comparison with *Shaker* channels. *Pflügers Arch.* 450:255–261.

Andersen, O.S., and S.W. Feldberg. 1996. The heterogeneous collision velocity for hydrated ions in aqueous solutions is  $\sim 10^4$  cm/s. *J. Physiol. Chem.* 100:4622–4629.

Armstrong, C.M., F. Bezanilla, and E. Rojas. 1973. Destruction of sodium conductance inactivation in squid axons perfused with pronase. *J. Gen. Physiol.* 62:375–391.

Baukowitz, T., and G. Yellen. 1996. Use-dependent blockers and exit rate of the last ion from a multi-ion pore of a  $K^+$  channel. *Science*. 271:653–656.

Beilby, M.J. 1985. Potassium channels at *Chara* plasmalemma. *J. Exp. Bot.* 36:228–239.

Bentrop, D., M. Beyermann, R. Wissmann, and B. Fakler. 2001. NMR structure of the “ball-and-chain” domain of KCNMB2, the  $\beta 2$ -subunit of large conductance  $Ca^{2+}$ - and voltage-activated potassium channels. *J. Biol. Chem.* 276:42116–42121.

Bernèche, S., and B. Roux. 2005. A gate in the selectivity filter of potassium channels. *Structure*. 13:591–600.

Bertl, A., C.L. Slayman, and D. Gradmann. 1993. Gating and conductance in an outward-rectifying  $K^+$  channel from the plasma membrane of *Saccharomyces cerevisiae*. *J. Membr. Biol.* 132:183–199.

Bezanilla, F., and C.M. Armstrong. 1972. Negative conductance caused by entry of sodium and cesium ions into the potassium channels of squid axons. *J. Gen. Physiol.* 60:588–608.

Blunck, R., J.F. Cordero-Morales, L.G. Cuello, E. Perozo, and F. Bezanilla. 2006. Detection of the opening of the bundle crossing in KcsA with fluorescence lifetime spectroscopy reveals the existence of two gates for ion conduction. *J. Gen. Physiol.* 128:569–581.

Blunck, R., U. Kirst, T. Riessner, and U.P. Hansen. 1998. How powerful is the dwell time analysis of multi-channel records? *J. Membr. Biol.* 165:19–35.

Brelidze, T.I., and K.L. Magleby. 2005. Probing the geometry of the inner vestibule of BK channels with sugars. *J. Gen. Physiol.* 126:105–121.

Brelidze, T.I., X. Niu, and K.L. Magleby. 2003. A ring of eight conserved negatively charged amino acids doubles the conductance of BK channels and prevents inward rectification. *Proc. Natl. Acad. Sci. USA*. 100:9017–9022.

Caceci, M.S., and W.P. Cacheris. 1984. Fitting curves to data—the simplex algorithm is the answer. *BYTE*. 5/84:340–362.

Capener, C.E., P. Proks, F.M. Ashcroft, and M.P.S. Sansom. 2003. Filter flexibility in a mammalian K channel: models and simulations of Kir6.2 mutants. *Biophys. J.* 84:2345–2356.

Catterall, W.A. 2000. From ionic currents to molecular mechanisms: the structure and function of voltage-gated sodium channels. *Neuron*. 26:13–25.

- Claydon, T.W., S.Y. Makary, K.M. Dibb, and M.R. Boyett. 2003. The selectivity filter may act as the agonist-activated gate in the G protein-activated Kir3.1/Kir3.4 K<sup>+</sup> channel. *J. Biol. Chem.* 278:50654–50663.
- Compoin, M., P. Carloni, C. Ramseyer, and C. Girardet. 2004. Molecular dynamics study of the KcsA channel at 2.0-Å resolution: stability and concerted motions within the pore. *Biochim. Biophys. Acta.* 1661:26–39.
- Cordero-Morales, J.F., L.G. Cuello, and E. Perozo. 2006a. Voltage-dependent gating at the KcsA selectivity filter. *Nat. Struct. Mol. Biol.* 13:319–322.
- Cordero-Morales, J.F., L.G. Cuello, Y. Zhao, V. Jogini, D.M. Cortes, B. Roux, and E. Perozo. 2006b. Molecular determinants of gating at the potassium-channel selectivity filter. *Nat. Struct. Mol. Biol.* 13:311–318.
- Cox, D.H., J. Cui, and R.W. Aldrich. 1997. Separation of gating properties from permeation and block in mslo large conductance Ca-activated K<sup>+</sup> channels. *J. Gen. Physiol.* 109:633–646.
- DeCoursey, T.E., S.Y. Kim, M.R. Silver, and F.N. Quandt. 1996. III. Ion channel expression in PMA-differentiated human THP-1 macrophages. *J. Membr. Biol.* 152:141–157.
- Del Camino, D., and G. Yellen. 2001. Tight steric closure at the intracellular activation gate of a voltage-gated K<sup>+</sup> channel. *Neuron.* 32:649–656.
- Del Camino, D., M. Holmgren, Y. Liu, and G. Yellen. 2000. Blocker protection in the pore of a voltage-gated K<sup>+</sup> channel and its structural implications. *Nature.* 403:321–325.
- Demo, S.D., and G. Yellen. 1992. Ion effects of gating of the Ca<sup>2+</sup>-activated K<sup>+</sup> channel correlate with occupancy of the pore. *Biophys. J.* 61:639–648.
- Draber, S., and U.P. Hansen. 1994. Fast single-channel measurements resolve the blocking effect of Cs<sup>+</sup> on the K<sup>+</sup> channel. *Biophys. J.* 67:120–129.
- Farokhi, A., M. Keunecke, and U.P. Hansen. 2000. The anomalous mole fraction effect in *Chara*: gating at the edge of temporal resolution. *Biophys. J.* 79:3072–3082.
- Feller, W. 1968. An Introduction to Probability Theory and Its Applications. Volume 1. John Wiley & Sons, Inc., New York.
- Ferguson, W.B. 1991. Competitive Mg<sup>2+</sup> block of a large-conductance, Ca<sup>2+</sup>-activated K<sup>+</sup> channel in rat skeletal muscle. *J. Gen. Physiol.* 98:163–181.
- FitzHugh, R. 1983. Statistical properties of the asymmetric random telegraph signal with application to single-channel analysis. *Math. Biosci.* 64:75–89.
- Fisahn, J., U.P. Hansen, and D. Gradmann. 1986. Determination of charge, stoichiometry and reaction constants from I-V curve studies on a K<sup>+</sup> transporter in *Nitella*. *J. Membr. Biol.* 94:245–252.
- Fujiwara, Y., and Y. Kubo. 2006. Functional roles of charged amino acid residues on the wall of the cytoplasmic pore of Kir2.1. *J. Gen. Physiol.* 127:401–419.
- Gradmann, D., H.G. Klieber, and U.P. Hansen. 1987. Reaction-kinetic parameters for ion transport from steady-state current-voltage curves. *Biophys. J.* 51:569–585.
- Green, W.N., and O.S. Andersen. 1991. Surface charges and ion channel function. *Annu. Rev. Physiol.* 53:341–359.
- Hansen, U.P. 1986. Reaction kinetic models of pumps, cotransporters and channels. In *Ion Channels and Electrogenic Pumps in Biomembranes. Abstracts of Lectures and Posters*, Osaka University. pp. L13–L33.
- Hansen, U.P., O. Cakan, M. Abshagen, and A. Farokhi. 2003. Gating models of the anomalous mole fraction effect of single-channel current in *Chara*. *J. Membr. Biol.* 192:45–63.
- Hansen, U.P., and J. Fisahn. 1987. I/V-curve studies of the control of a K<sup>+</sup>-transporter in *Nitella* by temperature. *J. Membr. Biol.* 98:1–13.
- Hansen, U.P., M. Keunecke, and R. Blunck. 1997. Gating and permeation models of plant channels. *J. Exp. Bot.* 48:365–382.
- Hansen, U.P., D. Gradmann, D. Sanders, and C.L. Slayman. 1981. Interpretation of current-voltage relationships for “active” ion transport systems: I. Steady-state reaction-kinetic analysis of Class-I mechanisms. *J. Membr. Biol.* 63:165–190.
- Hille, B. 1992. *Ionic Channels of Excitable Membranes*. Second edition. Sinauer Associates Inc., Sunderland, MA. 607 pp.
- Huang, Y., M.J. Lemieux, J. Song, M. Auer, and D.N. Wang. 2003. Structure and mechanism of the glycerol-3-phosphate transporter from *Escherichia coli*. *Science.* 301:616–620.
- Huth, T., I. Schroeder, and U.P. Hansen. 2007. The power of two-dimensional dwell-time analysis for model discrimination, temporal resolution, multi-channel analysis and level detection. *J. Membr. Biol.* 10.1007/s00232-006-0074-6.
- Immke, D., M. Wood, L. Kiss, and S.J. Korn. 1999. Potassium-dependent changes in the conformation of the Kv2.1 potassium channel pore. *J. Gen. Physiol.* 113:819–836.
- Jiang, X., A. Lee, J. Chen, M. Cadene, B.T. Chait, and R. MacKinnon. 2002. The open pore conformation of potassium channels. *Nature.* 417:523–526.
- Kahawara, K., M. Hunter, and G. Giebisch. 1990. Calcium-activated potassium channels in the luminal membrane of *Amphiuma* diluting segment: voltage-dependent block by intracellular Na<sup>+</sup> upon depolarization. *Pflügers Arch.* 416:422–427.
- Kang, M., A. Moroni, S. Gazzarini, D. DiFrancesco, G. Thiel, M. Severino, and J.L. Van Etten. 2004. Small potassium ion channel proteins encoded by *Chlorella* viruses. *Proc. Natl. Acad. Sci. USA.* 101:5318–5324.
- Khalili-Araghi, F., E. Tajkhorshid, and K. Schulten. 2006. Dynamics of K<sup>+</sup> conduction through Kv1.2. *Biophys. J.* 91:L72–L74.
- Kiss, T., J. LoTurco, and S.J. Korn. 1999. Contribution of the selectivity filter to inactivation in potassium channels. *Biophys. J.* 76:253–263.
- Klieber, H.-G., and D. Gradmann. 1993. Enzyme kinetics of the prime K<sup>+</sup> channel in the tonoplast of *Chara*: selectivity and inhibition. *J. Membr. Biol.* 132:253–265.
- Koval, O.M., Y. Fan, and B.S. Rothberg. 2007. A role for the S0 transmembrane segment in voltage-dependent gating of BK channels. *J. Gen. Physiol.* 129:209–220.
- Läuger, P., and G. Stark. 1970. Kinetics of carrier-mediated ion transport across lipid bilayer membranes. *Biochim. Biophys. Acta.* 211:458–466.
- Lehmann-Horn, F., and K. Jurkat-Rott. 1999. Voltage-gated ion channels and hereditary disease. *Physiol. Rev.* 79:1317–1372.
- LeMasurier, M., L. Heginbotham, and C. Miller. 2001. KcsA: it’s a potassium channel. *J. Gen. Physiol.* 118:303–313.
- Li, Y., I. Berke, L. Chen, and Y. Jiang. 2007. Gating and inward rectifying properties of the MthK K<sup>+</sup> channel with and without the gating ring. *J. Gen. Physiol.* 129:109–120.
- Liu, Y.S., P. Sompornpisut, and E. Perozo. 2001. Structure of the KcsA channel in the open state. *Nat. Struct. Biol.* 8:883–887.
- Loussouarn, G., E.N. Makhina, T. Rose, and C.G. Nichols. 2000. Structure and dynamics of the pore of inwardly rectifying K<sub>ATP</sub> channels. *J. Biol. Chem.* 275:1137–1144.
- Lu, R., A. Alioua, Y. Kumar, M. Eghbali, E. Stefani, and L. Toro. 2006. MaxiK channel partners: physiological impact. *J. Physiol.* 570:65–72.

- Lu, T., L. Wu, J. Xiao, and J. Yang. 2001a. Permeant-ion dependent changes in gating of Kir2.1 inward rectifier potassium channels. *J. Gen. Physiol.* 118:509–521.
- Lu, T., A.Y. Ting, J. Mainland, Y.G. Jan, P.G. Schultz, and J. Yang. 2001b. Probing ion permeation and gating in a K<sup>+</sup> channel with backbone mutations in the selectivity filter. *Nat. Neurosci.* 4:239–246.
- Lu, Z., and R. MacKinnon. 1994. A conductance maximum observed in an inward-rectifier potassium channel. *J. Gen. Physiol.* 104:477–486.
- Marty, A. 1983. Blocking of large unitary calcium-dependent potassium currents by internal sodium ions. *Pflugers Arch.* 396:179–181.
- Matteson, D.R., and R.P. Swenson. 1986. External monovalent cations that impede the closing by acting at a site in the channel. *J. Gen. Physiol.* 87:795–816.
- Melishchuk, A., A. Loboda, and C.M. Armstrong. 1998. Loss of *Shaker* K channel conductance in 0 K<sup>+</sup> solutions: role of the voltage sensor. *Biophys. J.* 75:1828–1835.
- Morais-Cabral, J.H., Y. Zhou, and R. MacKinnon. 2001. Energetic optimization of ion conduction rate by the K<sup>+</sup> selectivity filter. *Nature.* 414:37–42.
- Moss, G.W., and E. Moczydlowski. 1996. Rectifying conductance substates in a large conductance Ca<sup>2+</sup> activated K<sup>+</sup> channel: evidence for a fluctuating barrier mechanism. *J. Gen. Physiol.* 107:47–68.
- Murata, Y., Y. Fujiwara, and Y. Kubo. 2002. Identification of a site involved in the block by extracellular Mg<sup>2+</sup> and Ba<sup>2+</sup> as well as permeation of K<sup>+</sup> in the Kir2.1 K<sup>+</sup> channel. *J. Physiol.* 544:665–677.
- Nelson, P.H. 2002. A permeation theory for single-file ion channels: corresponding occupancy states produce Michaelis-Menton behaviour. *J. Chem. Physiol.* 117:11396–11403.
- Nimigeon, C.M., J.S. Chappie, and C. Miller. 2003. Electrostatic tuning of ion conductance in potassium channels. *Biochemistry.* 42:9263–9268.
- Nimigeon, C.M., and C. Miller. 2002. Na<sup>+</sup> block and permeation in a K<sup>+</sup> channel of known structure. *J. Gen. Physiol.* 120:323–335.
- Niu, X., X. Qian, and K.L. Magleby. 2004. Linker-gating ring complex as passive spring and Ca<sup>2+</sup>-dependent machine for a voltage- and Ca<sup>2+</sup>-activated potassium channel. *Neuron.* 42:745–756.
- Pagliuca, C., T.A. Goetze, R. Wagner, G. Thiel, A. Moroni, and D. Parcej. 2007. Molecular properties of Kcv, a virus encoded K<sup>+</sup> channel. *Biochemistry.* 46:1079–1090.
- Perozo, E., D.M. Cortes, and L.C. Cuello. 1999. Structural rearrangements underlying K<sup>+</sup> channel activation gating. *Science.* 285:73–78.
- Piskorowski, R.A., and R.W. Aldrich. 2006. Relationship between pore occupancy and gating in BK potassium channels. *J. Gen. Physiol.* 127:557–576.
- Proks, P., C.E. Capener, P. Jones, and F.M. Ashcroft. 2001. Mutations within the P-loop of Kir6.2 modulate the intraburst kinetics of the ATP-sensitive potassium channel. *J. Gen. Physiol.* 118:341–353.
- Proks, P., C. Girard, S. Haider, A.L. Gloyn, A.T. Hattersley, M.S.P. Sansum, and F.M. Ashcroft. 2005. A gating mutation at the internal mouth of the Kir6.2 pore is associated with the DEND syndrome. *EMBO Rep.* 6:470–475.
- Ransom, C.B., and H. Sontheimer. 2001. BK channels in human glioma cells. *J. Neurophysiol.* 85:790–803.
- Riessner, T. 1998. Level Detection and Extended Beta Distributions for the Analysis of Fast Rate Constants of Markov Processes in Sampled Data. Shaker-Verlag, Aachen, Germany. 74 pp.
- Riessner, T., F. Woelk, M. Abshagen-Keunecke, A. Caliebe, and U.-P. Hansen. 2002. A new level detector for ion channel analysis. *J. Membr. Biol.* 189:105–118.
- Roux, B. 2006. Extracellular blockade of potassium channels by TEA<sup>+</sup>: the tip of the iceberg? *J. Gen. Physiol.* 128:635–636.
- Sakmann, B., and G. Trube. 1984. Voltage-dependent inactivation of inward-rectifying single-channel currents in the guinea-pig heart cell membrane. *J. Physiol.* 347:659–683.
- Schroeder, I., and U.-P. Hansen. 2006. Strengths and limits of beta distributions as a means of reconstructing the true single-channel current in patch clamp time series with fast gating. *J. Membr. Biol.* 210:199–212.
- Schroeder, I., P. Harlfinger, T. Huth, and U.-P. Hansen. 2005. A subsequent fit of time series and amplitude histogram of patch clamp data reveals rate constants up to 1 μs<sup>-1</sup>. *J. Membr. Biol.* 203:83–99.
- Schroeder, I., T. Huth, V. Suitchmezian, J. Jarosik, S. Schnell, and U.-P. Hansen. 2004. Distributions-per-level: a means of testing level detectors and models of patch clamp data. *J. Membr. Biol.* 197:49–58.
- Schultze, R., and S. Draber. 1993. A nonlinear filter algorithm for detection of jumps in patch-clamp data. *J. Membr. Biol.* 132:41–52.
- Sørensen, J.B., M.S. Nielsen, C.N. Gudme, E.H. Larsen, and R. Nielsen. 2001. Maxi K channels co-localised with CFTR in the apical membrane of an exocrine acinus: possible involvement in secretion. *Pflugers Arch.* 442:1–11.
- Spruce, A.E., N.B. Standen, and P.R. Stanfield. 1989. Rubidium ions and the gating of delayed rectifier potassium channels of frog skeletal muscle. *J. Physiol.* 411:597–610.
- Swenson, R.P., and C.M. Armstrong. 1981. K<sup>+</sup> channels close more slowly in the presence of external K<sup>+</sup> and Rb<sup>+</sup>. *Nature.* 291:427–429.
- Tayefeh, S., T. Kloss, G. Thiel, B. Hertel, A. Moroni, and S.M. Kast. 2007. Molecular dynamics simulation of the cytosolic mouth in Kcv-type potassium channels. *Biochemistry.* 46:4826–4839.
- Tester, M. 1988. Blockade of potassium channels in the plasmalemma of *Chara corallina* by tetraethylammonium, Ba<sup>2+</sup>, Na<sup>+</sup> and Cs<sup>+</sup>. *J. Membr. Biol.* 105:77–85.
- Townsend, C., and R. Horn. 1999. Interaction between the pore and a fast gate of the cardiac sodium channel. *J. Gen. Physiol.* 113:321–331.
- Trapp, S., P. Proks, S.J. Tucker, and F.M. Ashcroft. 1998. Molecular analysis of ATP-sensitive K channel gating and implications for channel inhibition by ATP. *J. Gen. Physiol.* 112:333–349.
- Wang, Z., X. Zhang, and D. Fedida. 2000. Regulation of transient Na<sup>+</sup> conductance by intra- and extracellular K<sup>+</sup> in the human delayed rectifier K<sup>+</sup> channel Kv1.5. *J. Physiol.* 523:575–591.
- Weise, R., and D. Gradmann. 2000. Effects of Na<sup>+</sup> on the predominant K<sup>+</sup> channel in the tonoplast of *Chara*: decrease of conductance by blocks in 100 ns range and induction of oligo- or poly-subconductance gating modes. *J. Membr. Biol.* 175:87–93.
- Wood, M.J., and S.J. Korn. 2000. Two mechanisms of K<sup>+</sup>-dependent potentiation in Kv2.1 potassium channels. *Biophys. J.* 79:2535–2546.
- Xie, L.H., S.A. John, B. Ribalet, J.N. Weiss. 2004. Regulation of gating by negative charges in the cytoplasmic pore in the Kir2.1 channel. *J. Physiol.* 561:159–168.

- Yang, J., M. Yu, Y.N. Jan, and L.Y. Jan. 1997. Stabilization of ion selectivity filter by pore loop ion pairs in an inwardly rectifying potassium channel. *Proc. Natl. Acad. Sci. USA*. 94:1568–1571.
- Yeh, J.Z., and C.M. Armstrong. 1978. Immobilisation of gating charge by substance that simulates inactivation. *Nature*. 273:387–389.
- Yeh, S.H., H.K. Chang, and R.C. Shieh. 2005. Electrostatics in the cytoplasmic pore produce intrinsic inward rectification in Kir2.1 channels. *J. Gen. Physiol.* 126:551–562.
- Yellen, G. 1984. Ionic permeation and blockade in Ca<sup>2+</sup>-activated K<sup>+</sup> channels of bovine chromaffin cells. *J. Gen. Physiol.* 84:157–186.
- Yi, B.A., Y.-F. Lin, Y.N. Jan, and L.Y. Jan. 2001. Yeast screen for constitutively active mutant G protein-activated potassium channels. *Neuron*. 29:657–667.
- Zhang, Y., X. Niu, T.I. Brelidze, and K.L. Magleby. 2006. Ring of negative charge in BK channels facilitates block by intracellular Mg<sup>2+</sup> and polyamines through electrostatics. *J. Gen. Physiol.* 128:185–202.
- Zhao, Y., V. Yarov-Yarovoy, T. Scheuer, and W.A. Caterall. 2004. A gating hinge in Na<sup>+</sup> channels: a molecular switch for electrical signaling. *Neuron*. 41:859–865.
- Zheng, J., and F.J. Sigworth. 1997. Selectivity changes during activation of mutant *Shaker* potassium channels. *J. Gen. Physiol.* 110:101–117.
- Zheng, J., and F.J. Sigworth. 1998. Intermediate conductance during deactivation of heteromultimeric *Shaker* potassium channels. *J. Gen. Physiol.* 112:457–474.
- Zheng, J., L. Venkataramanan, and F.J. Sigworth. 2001. Hidden Markov model analysis of intermediate gating steps associated with the pore gate of *Shaker* potassium channels. *J. Gen. Physiol.* 118:547–562.
- Zhou, Y., and R. MacKinnon. 2003. The occupancy of ions in the K<sup>+</sup> selectivity filter: charge balance and coupling of ion binding to a protein conformational change underlie high conduction rates. *J. Mol. Biol.* 333:965–975.
- Zhou, Y., J.H. Morais-Cabral, A. Kaufman, and R. MacKinnon. 2001. Chemistry of ion coordination and hydration revealed by a K<sup>+</sup> channel-Fab complex at 2.0 Å resolution. *Nature*. 414:43–48.

Author: Read proofs carefully. This is your ONLY opportunity to make changes. No further alterations will be allowed after this point.

#### Author Queries

[AQ1] Please provide the total number of pages for this book.

**The Journal of General Physiology**  
**FIGURE APPROVAL**

Author:

MS#:

Embedded in your Rough Galley PDF are high resolution versions of your figure files. This is the only form of proof that you will see for the figures that will appear in your upcoming *JGP* article. The images in the PDF appear as they will in the final online version of your article. Note that colors must be converted to CMYK for the print version, and color shifts may occur. Our main concern is to retain your original RGB data, which can only be achieved in the online version. You will not receive a CMYK proof.

The embedded figures are your original files. The only changes you might notice should be dimensions, labeling, or arrangement of panels. Any color and grayscale should look exactly like or extremely close to your submitted files, though they have been compressed slightly to prevent unwieldy file size. If any figures need correction (if the message of your illustration is not conveyed on the figure proof, or if there is a labeling error), you must contact the Press office immediately.

RUP has placed your figures from the electronic files that you supplied, and we cannot be responsible for figure reproduction quality. Files must be prepared to journal specification if results are to meet your expectations. If reprocessing is required, you must supply the production office with a new high-quality file. \*\*Reprocessing may delay publication. Authors will be charged for reprocessing unless there has been an error introduced by RUP.\*\*

If you have any questions, please contact your Production Editor at 212-327-7940

**PLEASE SIGN EITHER A OR B**

**A.** I approve all figures in my article.

\_\_\_\_\_  
Signature

\_\_\_\_\_  
Date

**B (part I).** I do not approve figure number(s)\_\_\_\_\_. I have described in an attached letter precisely what is not conveyed, and I have provided a corrected file. I am aware reprocessing may cause a delay in publication.

\_\_\_\_\_  
Signature

\_\_\_\_\_  
Date

**B (part II).** Does the author want to see revised figures (please circle one)?      **Yes**      **No**

•If "yes," please supply the name and email address of an alternate at your institution who you've authorized to review your figures and give final approval/disapproval on your behalf. **If you are not available when your revised files are ready and if an alternate contact has not been provided, your article will be delayed.**

\_\_\_\_\_  
Alternate's Name

\_\_\_\_\_  
Phone

**Please SIGN and FAX this form WITH YOUR CORRECTED PROOFS to:**

*The Journal of General Physiology*

**Fax: 212-327-8513**

**Authorization of Publication Charges • *The Journal of General Physiology***

MS# \_\_\_\_\_ First Author \_\_\_\_\_

Month \_\_\_\_\_

Your signature is **required**.

Page charges, offprints, authors' alterations, and color (if any) authorized by:

✕ \_\_\_\_\_

signature of department head or fiscal officer

**Publication Charges**

**Page Charges:** \$95.00 per page (includes up to 5 pages of color).

**Alterations:** Avoid changes in proof. The cost of authors' alterations is \$4.00 per change and will be added to your invoice. Figure reprocessing at the author's request will be charged at \$55.00 per subject.

**Color Illustrations:** \$250.00 per page (beyond the first 5 pages of color).

**Terms: Cash...No Discount.**

Make out the institutional purchase order to The Rockefeller University Press to cover *all* your charges: page, color, offprints, and alteration – add "plus authors' alteration charges" to your purchase order. **Manuscript number, author name, and journal name must be on purchase order. Please do not prepay your charges;** an exact invoice will be sent to you by The Rockefeller University Press after your article has been published. Purchase orders with incorrect totals may not be processed and invoices may be sent directly to the corresponding author. Checks must be drawn in U.S. currency on an American bank. All checks must have micro-encoding on the bottom of the check. Make checks and purchase orders payable to:

**Rockefeller University Press, *Journal of General Physiology*, 1114 First Ave., New York, NY 10021-8325**

**Billing Instructions\*** (please print or type)

Page charges, offprints, alterations, and color (if any) are to be charged to:

Name: \_\_\_\_\_

Institution \_\_\_\_\_

Department \_\_\_\_\_

Street \_\_\_\_\_

City, State, Zip Code \_\_\_\_\_

✕ \_\_\_\_\_  
Signature required

Purchase Order No.: \_\_\_\_\_

**OR**

Card Number	_____
Expiration Date	_____
Cardholder	_____
Telephone Number	_____
Fax Number	_____
✕ _____	
Signature required	

MasterCard, VISA, American Express, and Discover accepted. You will be notified before your card is charged.

\*For split payment, please include a detailed cover letter.

Check one:  ORDERING OFFPRINTS — SEE PAGE 2  
 NO OFFPRINTS ARE BEING ORDERED

# Offprint Order Form • *The Journal of General Physiology*

MS# \_\_\_\_\_ First Author \_\_\_\_\_

Month \_\_\_\_\_

Offprints in multiples of 100 copies from the *Journal of General Physiology* must be ordered at the time the author returns the page proof. The minimum quantity for which orders will be accepted is 100 copies. Shipment will be made by the printer approximately 21 days after publication. Please note, we cannot deliver to P.O. Boxes. **Foreign postage will be assessed based on the weight and destination of the shipment.**

## Offprint Prices

Pages	1-4	5-8	9-12	13-16	17-20	21-24	25-28	29-32	33-36	37-40	Add'l for typeset covers*	Add'l for journal covers
100 copies	\$180	\$295	\$450	\$580	\$720	\$860	\$1,010	\$1,105	\$1,275	\$1,430	\$125	\$270
200 copies	285	440	655	860	1,070	1,300	1,505	1,650	1,930	2,155	170	380
Add'l 100s over 200	55	75	120	140	175	210	245	275	325	360	55	95

\*Please note: Typeset covers are plain paper, stapled to the offprint, that have the article title and authors' names on them.

## Order

Without covers \_\_\_\_\_

With covers \_\_\_\_\_  Typeset  Journal

TOTAL \_\_\_\_\_

**Do not delay ordering your offprints.** Orders must be in hand before the Journal goes to press. Please be sure the total order includes offprints for all co-authors who may want them. Orders received after the issue closes will incur a \$40.00 late fee. Complete and return by **fax** with your corrected page proof within 48 hours to:

**Fax: 212-327-8513**

## Shipping Instructions

Ship \_\_\_\_\_ copies with/without covers

Ship \_\_\_\_\_ copies with/without covers

Name \_\_\_\_\_

Name \_\_\_\_\_

Univ./Inst. \_\_\_\_\_

Univ./Inst. \_\_\_\_\_

Street \_\_\_\_\_

Street \_\_\_\_\_

\_\_\_\_\_

\_\_\_\_\_

City, State, Zip Code \_\_\_\_\_

City, State, Zip Code \_\_\_\_\_

\_\_\_\_\_

\_\_\_\_\_

Telephone \_\_\_\_\_

Telephone \_\_\_\_\_